Measurement of grid heat loading in a negative ion source for producing intense H^- ion beams by aperture displacement focusing technique

Cite as: Review of Scientific Instruments **72**, 3829 (2001); https://doi.org/10.1063/1.1405798
Submitted: 20 June 2001 • Accepted: 09 July 2001 • Published Online: 26 September 2001

T. Takayanagi, T. Ikehata, Y. Okumura, et al.

Measurement of grid heat loading in a negative ion source for producing intense H^- ion beams by aperture displacement focusing technique

T. Takayanagi[a] and T. Ikehata
Department of Electric and Electronic Engineering, Ibaraki University, Hitachi-shi, Ibaraki-ken 316-8511, Japan

Y. Okumura, K. Watanabe, M. Hanada, and T. Amemiya
Japan Atomic Energy Research Institute, Naka-machi, Naka-gun, Ibaraki-ken 311-0193, Japan

(Received 20 June 2001; accepted for publication 9 July 2001)

Heat loading of acceleration grids has been investigated using a JAERI 400 keV negative hydrogen ion source, which has a three-stage multiaperture accelerator. To investigate the effect of beamlet steering on the heat loading, the apertures in the grounded grid were displaced up to 5 mm. The steering angle increased linearly with the displacement distance of the grid. The obtained steering angle was 7.5 mrad at the displacement distance of 5 mm. It was confirmed that the steering angle agrees well with the thin lens theory. Degradation of beam optics due to the steering was not observed. The heat load of the grounded grid was scarcely changed up to the displacement distance of 2 mm and then increased from 2.5% to 8% of the total input power when the grid was displaced from 2.5 to 5 mm. Heat loads of the other unsteered grids were not changed. © *2001 American Institute of Physics.* [DOI: 10.1063/1.1405798]

I. INTRODUCTION

High power negative ion sources are required for neutral beam injection (NBI) systems in magnetically confined fusion devices. For the International Thermonuclear Experimental Reactor (ITER), for example, a high power negative ion source that can produce 1 MeV, 40 A H^-/D^- ion beams, has been designed.[1] The ion source has a multiaperture extractor/accelerator where 1280 holes are drilled over a wide extraction area of 580 mm×1552 mm.[2] It is necessary to converge the negative ion beam extracted from each extraction/acceleration hole (or beamlet) towards the limited area of an injection port of ITER.

Beamlet steering by aperture displacement is an effective method to converge the multiple beamlets, and is widely used in the NBI systems equipped with high power ion sources. Many studies on beamlet steering by aperture displacement have been reported.[3–7] However, those studies are for the positive ion sources that have a simple triode or tetrode extractor. The negative ion source has a more complicated extractor/accelerator to suppress the electron acceleration and to accelerate the negative ions to higher energy. Namely, permanent magnets are inserted in the extraction grid to deflect the extracted electrons, and the negative ions are accelerated up to, for example, 500 keV in JT-60[8] and 1 MeV in ITER[1] with a multistage accelerator. Only a few studies exist for the beamlet steering in the negative ion source.[9]

The negative ion source for JT-60 utilizes the aperture displacement technique to converge the beamlets extracted from 450 mm×1100 mm area. Maximum displacement distance of the apertures of 16 mm in diameter was 4.5 mm in the grounded grid. It was found that the heat load in the grounded grid was higher than the expected value. One of the reasons for the excessive heat load is considered to be the displacement of the apertures. However, no study exists for the heat load of the grid in the aperture displacement system. To design high power negative ion sources, it is very important to know the characteristics of the heat load when the apertures are displaced.

In the present article, experimental studies on the beamlet steering angle and the heat load of acceleration grids are reported.

II. EXPERIMENTAL APPARATUS AND MEASUREMENT

Figure 1 shows a cross sectional view of an experimental apparatus. A negative ion source, called JAERI 400 keV hydrogen negative ion source, has a multiaperture, three-stage accelerator.[10,11] The negative hydrogen ions (H^-) generated in a semicylindrical plasma generator called "KAMABOKO source"[12] are extracted and accelerated. A beam target plate made of tungsten is placed at 1.6 m downstream from the grounded grid (GRG). Dimensions of the target plate are 250 mm×250 mm, and 2 mm in thickness. Footprints of the accelerated beamlets are monitored with an infrared camera by observing the temperature rise of the target through the sapphire glass.[13] The spatial resolution of the infrared camera is about 0.5 mm.

A schematic of the negative ion extractor/accelerator and negative ion beam trajectory for single aperture is shown in Fig. 2. The extractor consists of three grids, called the plasma grid (PG), extraction grid (EXG), and electron suppression grid (ESG). The diameter of the apertures is 14 mm in PG. Thickness of PG, EXG, and ESG are 2 mm, 11 mm, and 3 mm, respectively. Distance between the grids is 6 mm

[a]Present address: NBI Heating Laboratory JAERI, 801-1 Mukoyama, Naka-machi, Naka-gun, Ibaraki-ken 311-0193, Japan; electronic mail: takayant@fusion.naka.jaeri.go.jp

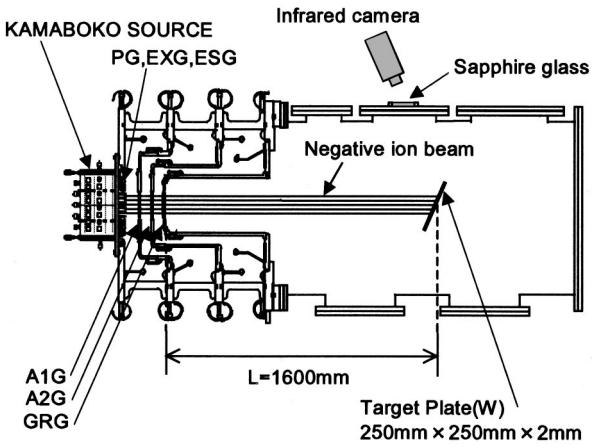

FIG. 1. Cross sectional view of an experimental apparatus is presented. A JAERI 400 keV negative ion source, which has multiaperture, three-stage accelerator, is installed. A target plate made of tungsten is placed at 1.6 m downstream from GRG. Footprints of the accelerated beamlets are monitored.

(PG-EXG) and 3 mm (EXG-ESG). The H^- ions produced in the KAMABOKO source are extracted by applying an extraction voltage between PG and EXG. ESG is electrically connected to EXG.

The accelerator consists of three grids, called first acceleration grid (A1G), second acceleration grid (A2G), and GRG. The diameter of the apertures is 16 mm. The thickness of the grids is 10 mm in the accelerator. The gap lengths are 75 mm (ESG-A1G), 65 mm (A1G-A2G), and 55 mm (A2G-GRG). The same voltage is applied for each acceleration stage. Therefore, the electrostatic field strength increases stage by stage to the downstream, forming an electrostatic lens. The negative ion beam is converged by the electrostatic lens.

Figure 3 shows the distribution of the apertures in the extractor. There are twenty-five (5×5) apertures for beam extraction and two apertures for detection of reference position. Permanent magnets are embedded between apertures rows in EXG to produce the dipole magnetic field for electron suppression.

In this experiment, GRG was displaced. Figure 4 shows a schematic of the beamlet steering by aperture displacement of GRG. A beamlet is steered using the electrostatic lens formed in GRG. Figure 5(a) is a photo of GRG taken from the ion source side. Figure 5(b) shows the opposite side. Twenty-five (5×5) apertures were displaced from an original

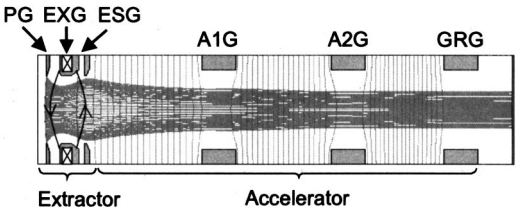

FIG. 2. Schematic of the negative ion acceleration equipment (extractor/accelerator) and negative ion beam trajectory for single aperture are shown. The diameter of the aperture is 14 mmφ in the extractor. The gap distance between PG and EXG and EXG and ESG are 6 mm and 3 mm, respectively. The diameter of the apertures is 16 mmφ and 10 mm thick in the accelerator. The gap distance is 75, 65, and 55 mm from the extractor side.

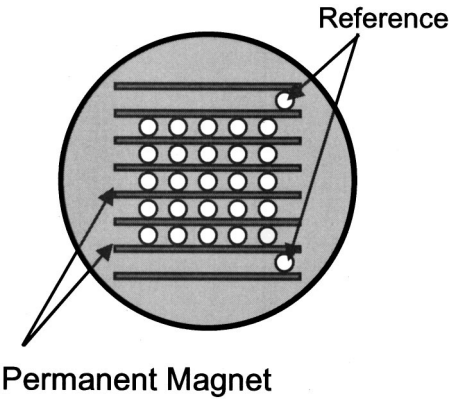

FIG. 3. Multiapertures distribution in EXG are shown. There are twenty-five (5×5) apertures for beam extraction and two apertures for reference. Permanent magnets are embedded between apertures row to suppress the electron extraction and acceleration.

position of 0 to 5 mm. Two additional apertures shown in Fig. 5(a) for the reference were not displaced. Beamlets extracted from these two apertures were used for the reference beamlets. The beamlet steering angle θ is defined as an Eq. (1).

$$\theta = \frac{\Delta d}{L}, \tag{1}$$

where Δd is a distance between the original position of the beamlet and the deflected position and L is a distance between GRG and the target. Beam steering angle was measured in the beam energy range from 70 to 140 keV.

Heat loads on each acceleration grid were measured by temperature rise of the cooling water.[10,11]

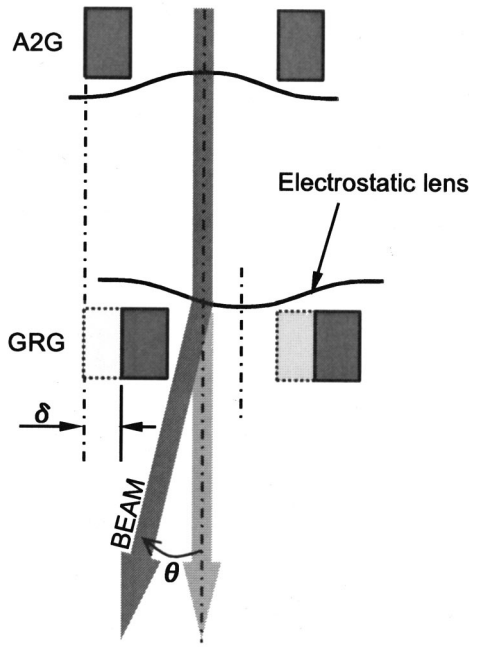

FIG. 4. Schematic of the beamlet steering by aperture displacement of GRG is shown. Beamlet is steered using the electrostatic lens formed in GRG.

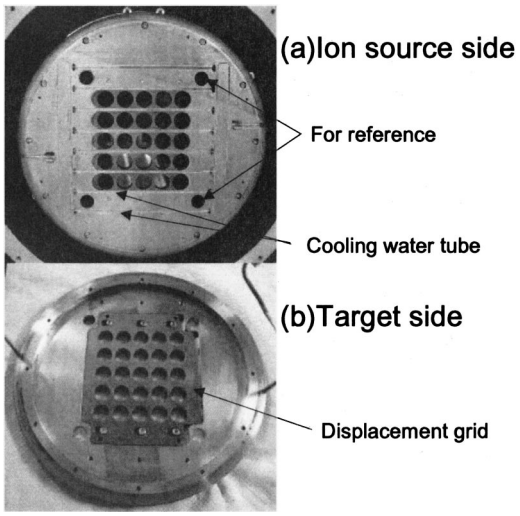

FIG. 5. Aperture displacement grid (GRG) for beamlet steering is shown. (a) is the ion source side and (b) is the target side. Twenty-five (5×5) apertures are displaced from an original position of 0 to 5 mm. Two additional apertures for the reference positioning are not displaced.

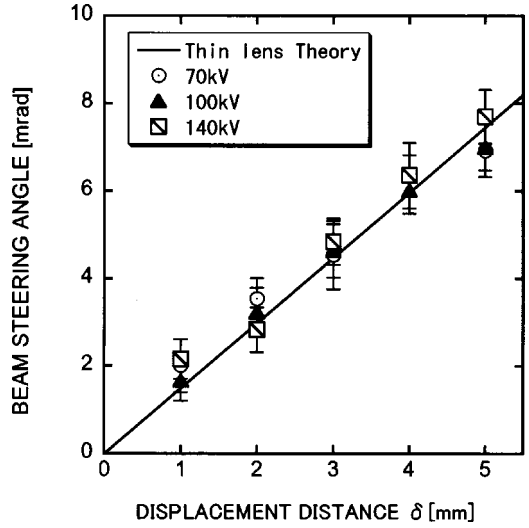

FIG. 7. Experimental results of beamlets steering angle and calculated results by thin lens theory are shown. The beamlet steering angle increases linearly with the aperture displacement distance in the beam energy range from 70 to 140 keV.

III. EXPERIMENTAL RESULTS AND DISCUSSION

A. Dependence of the beam steering angle on aperture displacement

Figure 6 shows an infrared image of the beamlet measured at the beam target. By optimizing beam optics, each beamlet was clearly observed. Adjacent beamlets rows were deflected alternately in the horizontal direction. This is due to the effect of the dipole magnetic field in the extraction grid. The outermost beamlets were deflected outward because of the beamlet–beamlet interaction.[13]

During the measurement of the steering angle, the magnetic field in EXG and the beam perveance were kept constant. The steering angle was measured by the distance between the original position of the beamlets and deflected beamlets. Therefore, influence of the magnetic field was eliminated in the measurement.

Figure 7 shows a result of the beamlet steering. The beamlet steering angle increased linearly as the aperture displacement distance increased from 0 to 5 mm. No dependence on the beam energy was observed between 70 and 140 keV. We confirmed that all the beamlets are steered with the same angle within the error bar for each corresponding displacement distance.

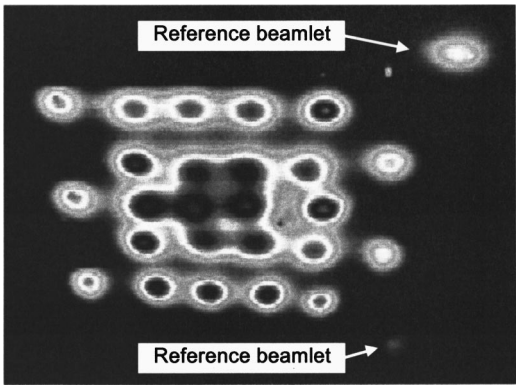

FIG. 6. Infrared image of the beamlets at beam target (The beam energy is 140 keV) is shown. By optimizing the beam optics, each beamlet is clearly observed. For the horizontal direction, adjacent beamlets rows deflect alternately. This phenomenon is due to the magnetic field in the extraction grid. The outermost beamlets are deflected outward of the beam.

In Fig. 7, the beamlet steering angle based on the thin lens theory[9] is also indicated. The steering angle θ is expressed as follows;

$$\theta = -\frac{E}{4V_{\mathrm{BE}}} \times \delta, \tag{2}$$

where V_{BE} is a total beam energy, and E is an electrostatic field strength between A2G and GRG. These experimental results agreed well with the thin lens theory.

A profile of an unsteered beam has been compared with the steered one. Figure 8(a) shows an infrared image of the beamlets. Beam energy was kept at 140 keV. The left-hand side image was measured for the displacement of 0 mm and the right-hand side one was measured for the displacement of 5 mm. No change in the beamlet image was observed.

To compare the beamlet profile in detail, beamlet profiles were described in Fig. 8(b). There was no change in temperature distribution of the beamlet core before or after the deflection. Beamlet profile deformation, which might be caused by a disturbance at the fringing electric field or the direct interception of the beamlet core, was not observed. The beamlet divergence $\omega(1/e)$ has been kept at about 5.5 mrad.

B. Heat load of acceleration grid

Figure 9 shows the heat load of GRG as a function of hydrogen gas pressure in the ion source. The measurement was performed for the displacement distances of 0 to 5 mm. The beam energy was kept at 90 keV. The gas pressure in the plasma generator was changed from 0.67 to 1.2 Pa, where the negative ion current was almost constant to keep the optimum beam optics. The heat load in the accelerator consists of two components; one is the heat load due to the direct interception of the beam, and the other is the heat load

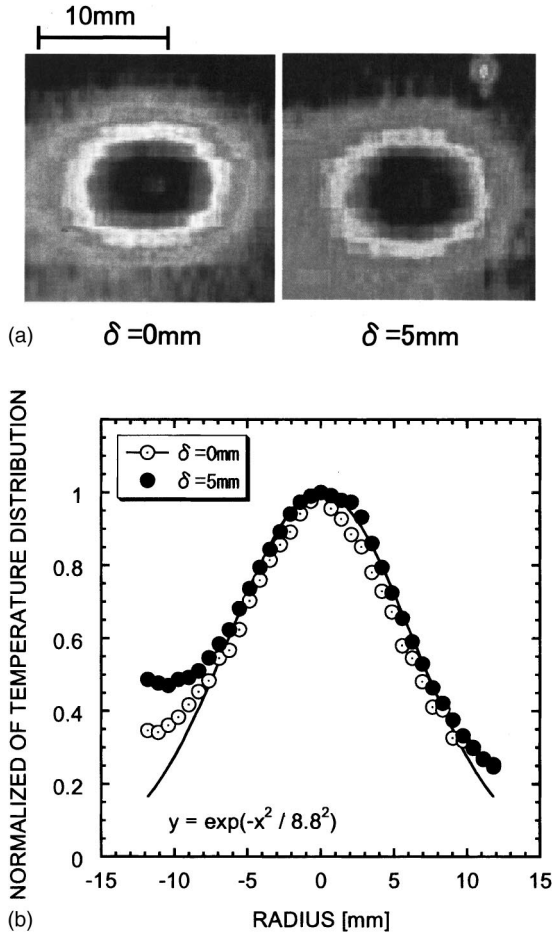

FIG. 8. (a) Beamlet images at the beam target measured with an infrared camera for the displacement distance (δ) of 0 and 5 mm are shown. The beam energy is 140 keV. (b) Temperature distribution (normalized) of the beamlets is shown. There is no change in temperature distribution of the beamlet core before or after deflection. The beamlet divergence $\omega(1/e)$ has been kept at about 5.5 mrad.

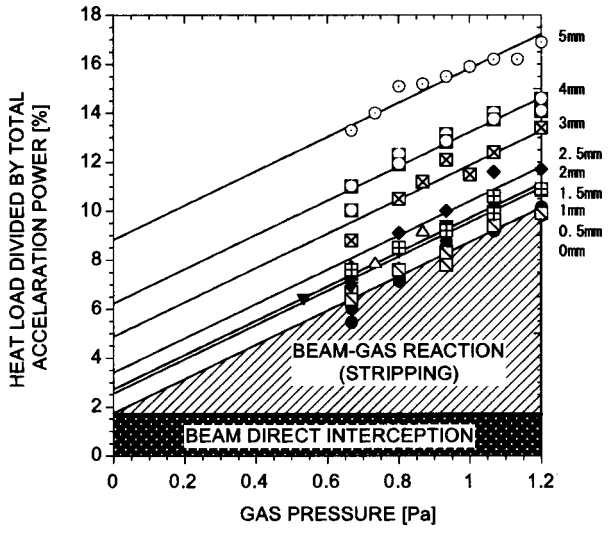

FIG. 9. Heat load of GRG as a function of hydrogen gas pressure in the ion source for various displacement distances of GRG is shown. The beam energy is kept at 90 keV. The change of gas pressure is from 0.67 to 1.2 Pa. The heat load due to the direct interception increases as a function of GRG displacement distance from 0 to 5 mm.

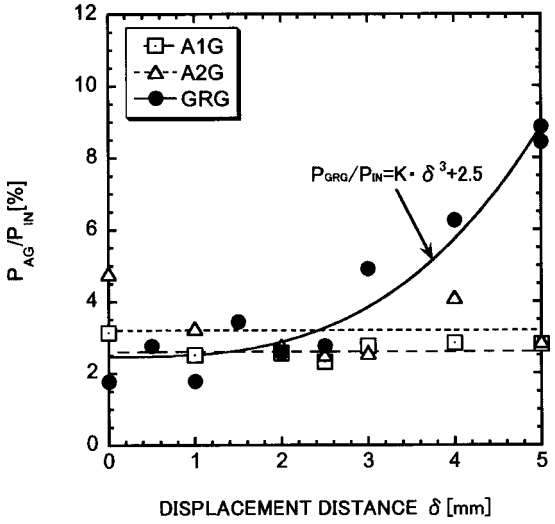

FIG. 10. Heat loads on each acceleration grids due to the direct interception as a function of GRG displacement distance are shown. The heat loads of A1G and A2G are constant during GRG displacement. The heat load of GRG increases as a function of displacement distance.

due to the beam–gas interaction, i.e., stripping of negative ions, in the accelerator. The direct interception does not change if the beam optics is kept constant. However, the stripping rate is strongly affected by residual gas pressure in the accelerator. The heat load caused by the striped electrons will increase with increasing gas pressure. The heat load due to the direct interception can be evaluated by extrapolating the heat load at the gas pressure of 0 Pa.[10,11]

Figure 10 shows the heat load on each acceleration grid due to the direct interception as a function of GRG displacement distance. We observed that the heat load due to the direct interception increased with increasing the displacement distance of the grid. The tendency of GRG heat load can be expressed by

$$P_{\mathrm{GRG}}/P_{\mathrm{IN}} = K \times \delta^3 + 2.5, \tag{3}$$

where $P_{\mathrm{GRG}}/P_{\mathrm{IN}}$ is the GRG heat load, K is the constant coefficient and δ is the displacement distance. 2.5 is the base of the heat load obtained without displacement, which is an interception. A solid line in Fig. 10 shows Eq. (3). Such a tendency of the heat loads can be explained as follows. A current density distribution of the beamlet is a Gaussian profile, as shown in Fig. 8(b). The experimental result showed that only the tail of the beamlet was intercepted. We assume that the tail is an edge of a simple cone profile. By displacement of the grid, the edge of the circular cone is scrapped. The scraped volume increases functionally to distance cubed (δ^3). The displacement distance of δ is the intercepted distance at the tail. The heat loads of A1G and A2G, which were not displaced, were constant at the same GRG displacement distance.

C. Heat load of GRG caused by beamlet deflections due to the dipole magnetic field in the extractor

As mentioned, the beamlet rows are deflected by the magnetic field in EXG. The influence of this deflection on the heat load was not clear. To clarify the relation between

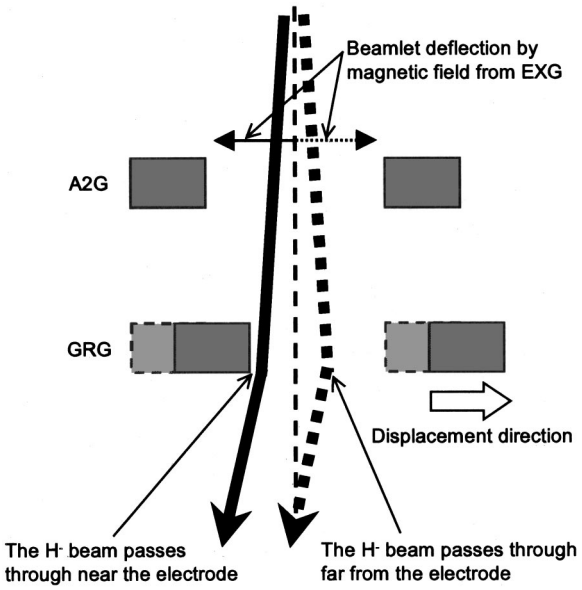

FIG. 11. Schematic of the two beamlet trajectories is shown. One beamlet passes through the hole near the electrode and the other passes through the hole far from the electrode by the effect of the magnetic field in the extractor when GRG is displaced.

the heat load and relative position of the beam trajectory to the grid aperture, we investigated the heat load on GRG. The beamlets were extracted from 5×5 apertures. Three rows of them were deflected in the same direction of the GRG displacement. The other two rows were deflected in the opposite direction of the GRG displacement. Figure 11 shows the schematic of beamlets for these two trajectories. One beamlet passes through the hole near the electrode and the other passes through the hole far from the electrode when GRG is displaced. To clarify the heat loads produced from these two kinds of beams, mask plates for PG were adopted. One plate covers the aperture of the beamlet passing through far from the grid; only 5×3 beamlets are extracted. The other plate covers the aperture of the beamlet passing near to the grid; only 5×2 beamlets are extracted, as shown in Fig. 12.

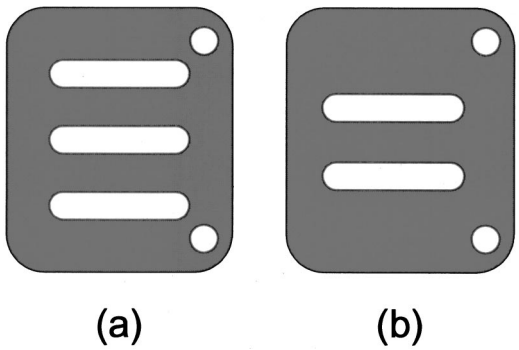

FIG. 12. Two mask plats for PG to clarify the heat loads produced from two kinds of beams are shown. The left-hand side plate (a) covers the aperture of beamlet passing through far from the grid; only 5×3 beamlets, which deflect in the same direction of the displacement, are extracted. The right-hand side plate (b) covers the aperture of beamlet passing near to the grid; only 5×2 beamlets, which deflect in the opposite direction of the displacement, are extracted.

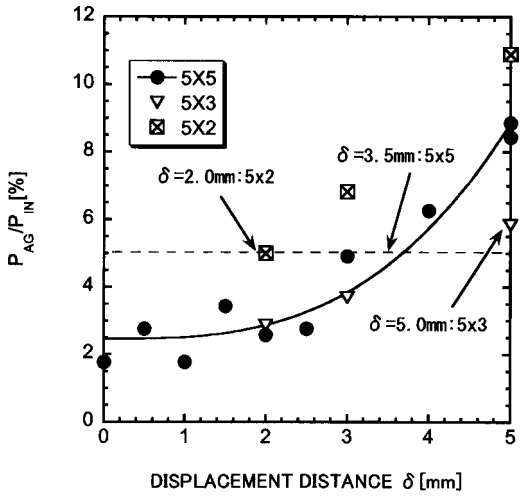

FIG. 13. Comparison of the heat loads measured with two PG masks and without mask (5×5 beamlets) are shown. Heat load measured for the 5×2 apertures is higher than that for the 5×5 apertures, while the heat load for 5×3 apertures shows lower value.

Figure 13 shows the comparison of the heat loads measured with two PG masks and without mask (5×5 beamlets). Heat load measured for the 5×2 apertures were higher than that for the 5×5 apertures, while the heat load for the 5×3 apertures showed lower value. The beamlet deflection angle due to the magnetic field in EXG is estimated about 0.9 mrad from the infrared image in Fig. 7. Therefore, the positions of the center of the beamlets are displaced by about 3 mm at the position of GRG. The heat load obtained using 5×2 apertures was about 5% at the displacement distance of 2 mm, which was almost the same as the heat load obtained using 5×3 apertures at the displacement distance of 5 mm. These experimental results agreed well with the estimation. We could confirm that the beamlets deflected by the dipole magnetic fields in the extractor and passing through near the displaced electrode (GRG) increase the heat load of GRG. This result shows that the heat load of GRG due to the beam deflection by the magnetic field in the extractor can be reduced lower than 2.5% by compensating the deflection.

[1] Y. Okumura, Y. Fujiwara, M. Kashiwagi, T. Kitagawa, K. Miyamoto, T. Morishita, H. Hanada, T. Takayanagi, M. Taniguchi, and K. Watanabe, Rev. Sci. Instrum. **71**, 1219 (2000).
[2] R. A. Hemsworth, Rev. Sci. Instrum. **67**, 1120 (1996).
[3] L. D. Stewart, J. Kim, and S. Matsuda, Rev. Sci. Instrum. **46**, 1193 (1975).
[4] J. H. Whealton, Rev. Sci. Instrum. **48**, 1428 (1977).
[5] J. R. Conrad, Rev. Sci. Instrum. **51**, 418 (1980).
[6] Y. Okumura, Y. Mizutani, and Y. Ohara, Rev. Sci. Instrum. **51**, 471 (1980).
[7] J. R. Conrad, Rev. Sci. Instrum. **51**, 1316 (1980).
[8] Y. Okumura, Y. Fujiwara, A. Honda, T. Inoue, M. Kuriyama, K. Miyamoto, N. Miyamoto, K. Mogaki, A. Nagase, Y. Ohara, K. Usui, and K. Watanabe, Rev. Sci. Instrum. **67**, 1018 (1996).
[9] T. Inoue, K. Miyamoto, A. Nagase, Y. Okumura, and K. Watanabe, JAERI-Tech 2000-023.
[10] K. Miyamoto, M. Hanada, T. Inoue, N. Miyamoto, A. Nagase, Y. Ohara, Y. Okumura, and K. Watanabe, 18th Symposium on Fusion Technology, Karlsruhe, Germany, 1994.
[11] M. Hanada, Y. Fujiwara, K. Miyamoto, Y. Okumura, and K. Watanabe, Rev. Sci. Instrum. **69**, 947 (1998).
[12] M. Hanada, T. Inoue, M. Mizuno, Y. Ohara, Y. Okumura, Y. Suzuki, H. Tanaka, M. Tanaka, and K. Watanabe, Rev. Sci. Instrum. **64**, 2699 (1992).
[13] Fujiwara, M. Hanada, Y. Okumura, and K. Watanabe, Rev. Sci. Instrum. **71**, 3059 (2000).